THE JOURNAL OF PHYSICAL CHEMISTRY B
A JOURNAL OF THE AMERICAN CHEMICAL SOCIETY

pubs.acs.org/JPCB

Article

Water-in-Salt: Fast Dynamics, Structure, Thermodynamics, and Bulk Properties

Laura Kacenauskaite,[§] Stephen J. Van Wyck,[§] Max Moncada Cohen, and Michael D. Fayer*

Cite This: *J. Phys. Chem. B* 2024, 128, 291−302

Read Online

ACCESS | Metrics & More | Article Recommendations | Supporting Information

ABSTRACT: We present concentration-dependent dynamics of highly concentrated LiBr solutions and LiCl temperature-dependent dynamics for two high concentrations and compare the results to those of prior LiCl concentration-dependent data. The dynamical data are obtained using ultrafast optical heterodyne-detected optical Kerr effect (OHD-OKE). The OHD-OKE decays are composed of two pairs of biexponentials, i.e., tetra-exponentials. The fastest decay (t_1) is the same as pure water's at all concentrations within error, while the second component (t_2) slows slightly with concentration. The slower components (t_3 and t_4), not present in pure water, slow substantially, and their contributions to the decays increase significantly with increasing concentration, similar to LiCl solutions. Simulations of LiCl solutions from the literature show that the slow components arise from large ion/water clusters, while the fast components are from ion/water structures that are not part of large clusters. Temperature-dependent studies (15−95 °C) of two high LiCl concentrations show that decreasing the temperature is equivalent to increasing the room temperature concentration. The LiBr and LiCl concentration dependences and the two LiCl concentrations' temperature dependences all have bulk viscosities that are linearly dependent on τ_c^{slow}, the correlation time of the slow dynamics (weighted averages of t_3 and t_4). Remarkably, all four viscosity vs $1/\tau_C^{slow}$ plots fall on the same line. Application of transition state theory to the temperature-dependent data yields the activation enthalpies and entropies for the dynamics of the large ion/water clusters, which underpin the bulk viscosity.

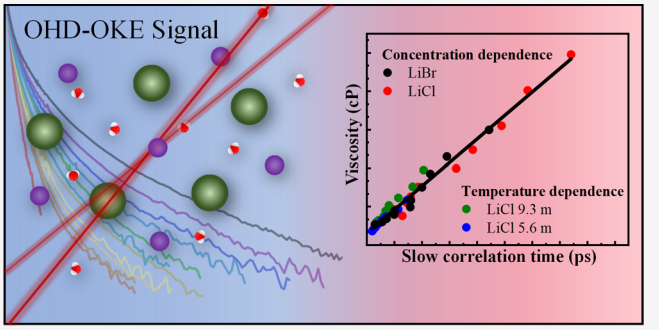

1. INTRODUCTION

The characteristics of ionic solutions are significant in chemistry, biology, and geology.[1−3] They are also the basis of technological progress for applications like water treatment facilities or safe and efficient energy storage and conversion systems.[4] The properties of water are closely related to the physical properties of the individual molecules and the structure and dynamics of water's hydrogen bonding network, which has been extensively studied using a variety of techniques.[5−9] The addition of salts to water modifies the hydrogen bonding in proximity to the ions and has a major impact on its molecular structure, dynamics, and bulk physicochemical properties.

The effects of ions on aqueous solutions, particularly at very high concentrations, is an area of substantial ongoing research.[10−16] At very high salt concentrations, the ions are not fully solvated and isolated from each other. Rather, they form ion/water clusters and, at the highest concentrations, extended ion/water networks, which are not thoroughly understood.[17−21]

For low ion concentrations, less than ∼0.1 M, accurate predictions of ionic solution properties can often be obtained from models based on the Debye−Huckel theory.[22,23] At higher concentrations (greater than ∼1 M), however, analytical theories that describe the complex nature of ionic solutions are lacking.[22,24] This is especially true for the very high concentration regime, often referred to as "water-in-salt" electrolytes, which can have as few as three water molecules per ion pair.[4,25−27] Recent theoretical investigations of the structure and dynamics of water-in-salt solutions include molecular dynamics (MD) simulations based on optimized force fields,[11,28,29] ab initio neural network-based deep potential MD, and density functional theory simulations.[30,31] These methods predict that most salinity effects arise from the clustering of salt ions, which disrupt the water hydrogen bonding network at high salt concentrations.

Although simulations have had success in reproducing some types of structural experimental data for moderate to high concentrations of some simple salts, limitations still arise when analyzing dynamics and the effects of alkali cations. Current

Received: November 22, 2023
Revised: November 30, 2023
Accepted: December 1, 2023
Published: December 20, 2023

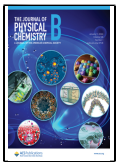

methods have less success in reproducing experimentally observed properties of highly concentrated lithium and sodium salts.[11]

Explicating how high ion concentrations affect bulk properties, such as viscosity, conductivity, and vapor pressure, is particularly challenging due to the lack of experimental methods to directly observe molecular level dynamics and relate them to bulk properties.[23,32] Various experimental techniques, including Raman spectroscopy,[33−37] depolarized Rayleigh scattering,[36,38] nuclear magnetic resonance,[39] X-ray and neutron scattering,[40] dielectric spectroscopy,[41−43] and ultrafast infrared (IR) spectroscopy,[17−19,44,45] have been employed to investigate the interactions between ions and water. X-ray and neutron scattering techniques are very useful for obtaining information about structures in concentrated salt solutions but do not provide information about their temporal evolution. NMR spectroscopy has made important contributions through the characterization of salt solutions on microsecond to millisecond time scales. However, NMR can only address faster dynamics indirectly.[46] Two-dimensional IR spectroscopy and other ultrafast IR methods have the necessary time resolution, but these methods can be limited by the vibrational lifetime of the probe vibration, e.g., water hydroxyl stretching mode, and are only sensitive to dynamics coupled to the probe vibration.[17,47] While OHD-OKE experiments cannot discriminate among chemical moieties, they measure dynamics of all structural components of salt solutions on all time scales because it is a nonresonant method that does not involve an excited state lifetime.

The various techniques have provided a great deal of information on concentrated salt solution properties, e.g., ion pairing and formation of specific hydration shells; however, they still do not address connections between microscopic dynamics and bulk properties.[48] Progress in this field will form the foundation for a fundamental understanding of ion/water interactions and enable technological advances in, e.g., high-energy-density and long-cycle-life batteries and more efficient ion-exchange membranes.

Here, we focus on selected lithium halide solutions due to their very high solubilities, substantial differences in the cation and anion sizes and charge densities, and their use as model systems related to potential applications. While LiBr and LiCl are quite similar, the ionic volume of bromide is 26% larger than that of chloride, and the sizes of ions have been shown to have a substantial impact on solution properties.[49−51] Small ions with high charge densities can more readily order water molecules in their solvation shell. Monoatomic alkali halide salts are often used to study ion size effects because of their simplicity.[13,35,52−54] A large difference between the size of the cation and anion results in alkali halide salts with very high solubilities.[51] For example, LiF is composed of two small ions, and it is only sparingly soluble (<0.1 m), while replacing the Li^+ with the much larger Cs^+ leads to remarkable solubility in water (~30 m).[55] Highly soluble lithium halide salts have been the subject of many studies because of their potential, but still limited, applicability in energy storage technology.[14,36,56,57]

One of the main drawbacks of lithium-ion batteries is their restricted temperature operating range, approximately −20 to 55 °C, which significantly limits their performance and imposes threats of spontaneous combustion or release of hazardous gases. Highly concentrated salt lithium-ion-based batteries have been shown to almost double the operating temperature range with improved stability and performance.[4,58,59] A molecular description of these phenomena is yet to be elucidated; therefore, better insights on how temperature affects ion mobility, viscosity, and proton transfer are important in this field.[60]

We present the results of experiments conducted with the optical heterodyne-detected optical Kerr effect (OHD-OKE) method. This nonresonant ultrafast experimental technique provides information about the structural dynamics of the entire ion/water system. It has been used to study a variety of aqueous systems,[61−63] including work by Heisler and co-workers who previously employed OHD-OKE to study the anion size effect in aqueous halide solutions.[64] However, their choice of sodium salts limited their investigation to moderately high concentrations. Turton et al. investigated eutectic LiCl solutions; OKE experiments were performed only in a low-temperature range (130−300 K) with a focus on the properties of supercooled liquids.[65]

These earlier OKE experiments, supported by MD simulations and frequency domain dielectric relaxation measurements, provided a good background for interpreting the molecular motions and relaxations that contribute to different time scale signals. The fastest, tens of femtoseconds to hundreds of femtoseconds, dynamics in the aqueous solutions are assigned to broad frequency distributions of librational motions of water molecules as well as transverse and longitudinal acoustic and optical phonon modes of the liquids, akin to true phonon modes of crystals.[66] These measurements provide high-frequency densities of the states of these modes. These types of 100 fs time scale dynamics do not provide information about ion/water structural reorganization dynamics, which occur on slower but still fast time scales. Longer decay time scales correspond to structural relaxation of ion/water structures, with water molecules forming a component of large ion/water clusters in highly concentrated solutions.[62,65,67]

In this study, we examine and compare the dynamics of LiBr to those of LiCl solutions[62] over a broad concentration range, i.e., 0.06−0.36 ion mole fraction (IMF) (1−29 to 1−3 salt ion pair-to-water molecule, ~2−15 m). In addition, we present temperature-dependent results on LiCl dynamics. Two concentrations, 1−10 and 1−6, were studied from 15 to 95 °C.

Based on previously published MD simulations of the concentration-dependent LiCl/water structures,[67] we associate the types of ion/water structures that give rise to the LiCl-specific dynamics,[62] and because of the similarities in the data, also to LiBr. Furthermore, the bulk viscosities as a function of the LiCl concentration are directly related to the slow correlation times τ_C^{slow} (the amplitude-weighted average of the two longest time constants), which characterize the dynamics of the large ion/water clusters. As with the concentration-dependent data of LiCl and LiBr, the temperature-dependent bulk viscosities of the two concentrations of LiCl track τ_C^{slow}. A remarkable result of this study is the bulk viscosity vs τ_C^{slow} for the concentration dependences of LiCl and LiBr solutions and the temperature dependences of LiCl solutions all fall on the same line. In addition, simple transition state theory[68] is used to relate $1/\tau_C^{slow}$ to the activation free energies, ΔG^*, for the two concentrations and to obtain their activation enthalpies and entropies, ΔH^* and ΔS^*.

2. EXPERIMENTAL PROCEDURES

2.1. Sample Preparation. Lithium bromide and lithium chloride (anhydrous, >99%) were acquired from Sigma-Aldrich. Deionized ultrafiltered water was acquired from

https://doi.org/10.1021/acs.jpcb.3c07711
J. Phys. Chem. B 2024, 128, 291−302

Fisher. All materials were used as received. The sample concentrations were prepared gravimetrically at room temperature. For the concentration-dependent studies, the samples were filtered through a 0.02 μm filter into a 1 cm path length glass cuvette for higher concentrations, ≥4 m, and into a 4 cm glass cell for the lower concentrations, <4 m. The cells were sealed with Teflon stoppers. All the concentration-dependent experiments were performed at 24.4 °C. The temperature-dependent experiments used a thermally insulated 5 cm long glass cell. A thermometer under the insulation in thermal contact with the cell and a temperature controller were used to set the temperature. The temperature was controlled to ±0.1 °C.

Experimental bulk viscosity values of LiCl and LiBr solutions used in this paper were obtained from the literature.[69] Some values for 1−10 LiCl solutions were determined by extrapolation (see Supporting Information (SI), Section I and Figure S1).

2.2. OHD-OKE Experimental Setup. The OHD-OKE experiment measures the time derivative of the polarizability−polarizability correlation function, which depends on the polarizability anisotropy.[70,71] The data are converted to the polarizability−polarizability correlation function by integration. The polarizability−polarizability correlation function reports on the structural dynamics of the ion/water systems. As the OHD-OKE is a nonresonant technique, it provides the ground state thermal equilibrium dynamics.

The electric field of the pump induces an oscillating polarization along a direction determined by the local anisotropic polarizability of the ion/water structures. The induced oscillating dipole of the local structures couples to the pump pulse's electric field and produces a minute structural modification, resulting in a small shift of the polarizability toward the direction of the pulse's electric field. The alignment causes temporary birefringence in the sample, which decays due to the dynamical relaxation and eventual randomization of the ion/water structures. The resulting signal[72−74] provides the polarizability−polarizability correlation function. Linear response theory[75] states that a system, initially in thermal equilibrium, will relax from a small perturbation by the system's thermal equilibrium fluctuations. Therefore, the time-dependent polarizability−polarizability correlation function provides the thermal equilibrium structural dynamics of the salt solutions.

The OHD-OKE experimental system has been described in detail previously.[76,77] The key elements are described here. Ultrafast pulses were generated by a 90 MHz Ti:sapphire oscillator, which was used to seed a 5 kHz Ti:sapphire regenerative amplifier. Pulse duration was adjusted to be ∼200 fs for the shorter time data and 2.5 ps (fwhm) for the longer time data by using a linear chirped pulse compressor. Using longer pulses for the slower decaying portion of the data improves the signal-to-noise ratio. An intense pump and weaker probe pulse were produced using a 98 and 2% beam splitter. The linearly polarized pump pulse introduced a transient birefringence along the axis of its electric field vector. The weaker probe pulse, with polarization set at 45° to the pump pulse, was used to measure the birefringence. The probe is passed through crossed polarizers: one before and one after the sample. Therefore, the extent of depolarization caused by the induced birefringence is measured.

To improve the signal-to-noise and reduce the interference from scattered pump light, heterodyne detection with phase and polarization cycling in a four-shot sequence at 1.25 kHz were used.[63] A balanced detector photodiode pair was used. The reference pulse's amplitude was adjusted to eliminate the local oscillator intensity, leaving the heterodyned signal, which was measured by a lock-in amplifier at 1.25 kHz. The timing of the probe pulse was controlled by using a computer-operated delay stage. The pump intensities were adjusted until no dependence on the pump power was observed.

3. RESULTS AND DISCUSSION

A. Anion Influence on Concentration-Dependent Dynamics. The OHD-OKE data were fit with tetra-exponential decay functions:

$$r(t) = R'(t) = A_1\exp(-t/t_1) + A_2\exp(-t/t_2) + A_3\exp(-t/t_3) + A_4\exp(-t/t_4) \quad (1)$$

where $R'(t)$ is the decaying OHD-OKE signal (the derivative of the polarizability−polarizability correlation function), the t_i's are the decay time constants, and A_i's are the associated amplitudes. The tetra-exponential is composed of two pairs of biexponential fast decay components (t_1 and t_2) related to those of pure water and slow decay components (t_3 and t_4) that do not occur in pure water, as discussed in detail below. This fitting model was chosen as it is the simplest model that results in a satisfactory fit. This multiexponential decay model has been shown to provide a direct physical and quantitative description of the structures in LiCl salt solutions and can be correlated with the bulk viscosity.[62]

The polarizability−polarizability correlation is obtained by the integration of eq 1:

$$R(t) = A_1t_1\exp(-t/t_1) + A_2t_2\exp(-t/t_2) + A_3t_3\exp(-t/t_3) + A_4t_4\exp(-t/t_4) \quad (2)$$

Because the sign of the signal in the experiments is arbitrary, we take $R(t)$ to be positive. The prefactors in eq 2 can be normalized and relabeled in the following manner:

$$C_1 = \frac{A_1t_1}{A_1t_1 + A_2t_2 + A_3t_3 + A_4t_4}$$

$$C_2 = \frac{A_2t_2}{A_1t_1 + A_2t_2 + A_3t_3 + A_4t_4}$$

$$C_3 = \frac{A_3t_3}{A_1t_1 + A_2t_2 + A_3t_3 + A_4t_4}$$

$$C_4 = \frac{A_4t_4}{A_1t_1 + A_2t_2 + A_3t_3 + A_4t_4} \quad (3)$$

The C_i's sum to 1 and represent the fractional amplitude, i.e., the normalized relative contribution associated with each time component.

OHD-OKE data for concentrated aqueous LiBr solutions were collected from 1−3.6 to 1−29 LiBr−water ratio (IMF of 0.36−0.06, 15.5−1.9 m). Figure 1A shows the OHD-OKE signal decays from a subset of the LiBr concentrations, including pure water. The decays for all the concentrations studied can be found in the SI, Figure S2. The data show that the observed dynamics slow with increasing LiBr concentration.

https://doi.org/10.1021/acs.jpcb.3c07711
J. Phys. Chem. B 2024, 128, 291−302

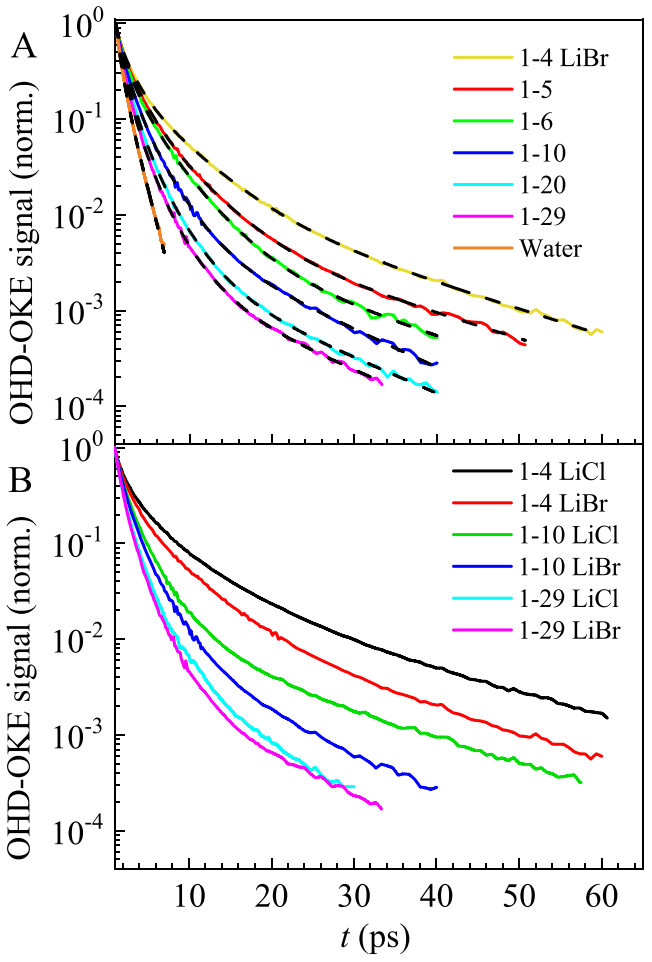

Figure 1. OHD-OKE signal decays of water and aqueous LiBr and LiCl solutions. The concentrations are given as 1 ion pair-number of water molecules. (A) OHD-OKE signal decays of pure water and moderate to high concentrations of LiBr (solid, colored curves). The dashed black curves are tetra-exponential decay fits to the data, except for water, which is a biexponential. Water data were reproduced from the literature.[62] (B) OHD-OKE signal decays of LiBr and LiCl solutions at variety of selected concentrations (solid, colored curves). LiCl data were reproduced from the literature.[62] The decays were normalized at 1 ps.

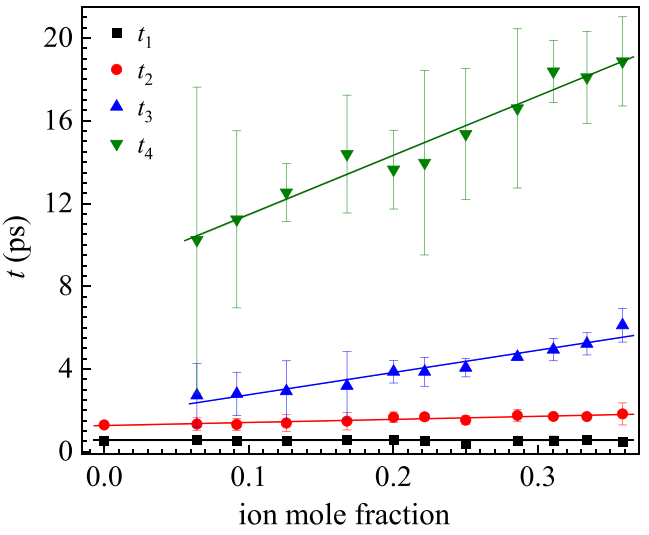

Figure 2. Four time constants, t_1 (black points), t_2 (red points), t_3 (blue points), and t_4 (green points), from the fits to the OHD-OKE data as a function of ion mole fraction of LiBr in water. The lines through the data are linear fits. If error bars are not visible, they are smaller than the symbol. t_1 is constant with the pure water value within experimental error. t_2 has a mild concentration dependence, increasing slightly from its pure water value. The t_1 and t_2 points at IMF = 0 are the pure water values. t_3 and t_4 have no counterparts in pure water. They are considerably slower than t_1 and t_2 and have much steeper concentration-dependent slopes.

Figure 1B shows a subset of the LiBr samples compared with previously published LiCl data.[62] For a given salt-to-water ratio, dynamics in LiBr solutions are consistently faster. Figure 2 and Table S2 in the SI show the four time constants as a function of LiBr concentration. As reported previously,[62,78−80] the pure water curve (see Figure 1A) decays as a biexponential, with the time constants t_1 = 0.52 ± 0.05 ps and t_2 = 1.29 ± 0.1 ps. As can be seen in Figure 2, black points, t_1 = ∼0.5 ps at all concentrations within experimental error. (All points in Figure 2 have error bars. If they are not visible, they are the size of the symbol or smaller.) t_2 (red points) increases very gradually across the concentration range studied. The slope of the linear fit is 1.5 ps/IMF. At the lowest several concentrations ∼1.3 ps within experimental error. At the highest concentration, t_2 slows to ∼1.8 ps at a 0.36 IMF (15.5 m). Therefore, t_1 has the pure water value at all concentrations studied within error, and t_2 increases slightly from its pure water value.

2D IR experiments have been previously used to determine the H-bond dynamics of pure water. The 2D IR measured decay of the frequency−frequency correlation function is biexponential with time constants, 0.4 ± 0.1 ps and 1.7 ± 0.1 ps.[7,81,82] These fast and slow time constants are assigned to local H-bond fluctuations and the randomization of the H-bond network, respectively.[7,81,82] 2D IR and OHD-OKE measure different correlation functions of the dynamics of the same system. 2D IR measures the time dependence of structural changes that influence the frequency of the vibrational probe molecule. For water, this is the OD stretch of dilute HOD in H_2O. OHD-OKE measures structural changes that influence the polarizability of the system. Both experiments are third-order nonlinear experiments that reflect the structural dynamics. For the same processes, the time constants will likely be similar. Therefore, it is reasonable to assign the two fast time constants (t_1 and t_2) to H-bond dynamics.

At the lowest concentration studied, IMF = 0.066, there are 29 water molecules per ion pair. In this solution, there will be some water molecules that are H-bonded only to other water molecules. There will also be water molecules that form the solvation shells of isolated ions. The simulations from the literature,[67] discussed in detail below, show that for our lowest concentration, ∼20% of the ions are in contact ion pairs. There may also be some solvent-separated ion pairs. LiCl forms contact ion pairs.[67] The similarities between the LiBr and LiCl data, described in detail below, indicate that LiBr mainly forms contact ion pairs.

The dynamical processes that contribute to t_1 and t_2 have a variety of structural origins. If the correlations with the 2D IR experiments are correct, the results show that within error (±0.1 ps for t_1), the H-bond length fluctuations are so similar for pure water-like structures, water solvating isolated ions, and water solvating contact ion pairs that the fluctuations average to the pure water value within the error. There will be no pure

https://doi.org/10.1021/acs.jpcb.3c07711
J. Phys. Chem. B 2024, 128, 291−302

water-like H-bonding except for the lowest two concentrations. At higher concentrations, the isolated solvated ions will decrease and be replaced by contact ion pairs and larger ion/water clusters. t_2 gradually slows with an increasing concentration. If t_2 is caused by H-bond rearrangements, as suggested by the 2D IR, then different environments could produce different but similar time constants. These dynamics would still give data with the appearance of a single time constant, t_2. If the water H-bond rearrangements are slower for contact ion pairs than for isolated solvated ions, which are slower than for pure water-like structures, t_2 will slow as the concentration of contact ion pairs grows at the expense of the other structures.

For LiBr, t_3 (blue points) and t_4 (green points) have much steeper slopes than the faster two time constants, 10.7 and 28.7 ps/IMF, respectively (see Figure 2). The values approximately double from the lowest to the highest ion concentrations, t_3 slowing from ∼2.5 to ∼6 ps and t_4 from ∼9 to ∼19 ps. In contrast to t_1 and t_2, the slower components have significant concentration dependencies. As discussed below, t_3 and t_4 can reasonably be associated with the dynamics of large ion/water clusters.

t_1 and t_2 have counter parts in pure water, while t_3 and t_4 do not. t_1 and t_2 are fast and have no or a very mild change with concentration, respectively. t_3 and t_4 are much slower and have significant slopes. We will divide the dynamics into two types, fast and slow, which will be associated with different ion/water structures in connection with the literature simulation results presented below. The sum of the fractions of these pairs of polarization correlation function decays (eq 3) $C_{fast} = C_1+C_2$ and $C_{slow} = C_3+C_4$, for LiBr (black) and LiCl (red),[62] are shown in Figure 3A (see Table S3 for values). The lines are linear fits to the data. As the IMF increases, the fraction C_{fast} decreases, and the fraction C_{slow} increases. While the slopes of the LiBr and LiCl lines differ, the basic trends are the same. The effective ionic radius of bromide is 8% larger than chloride, which leads to a 26% increase in volume.[83] As they both have a charge of −1, bromide will have a correspondingly lower charge density. The lower charge density of Br^- may contribute to a less rapid change from fast to slow contributions to the decay as the concentration increases.

The fractions of C_{fast} and C_{slow} in LiCl solutions as a function of concentration (squares) are compared with previously published MD simulations of concentrated LiCl solutions (circles).[67] The results are shown in Figure 3B. The simulations used concentration-dependent radial distribution functions with comparisons to X-ray and neutron scattering data[67] to determine the fraction of ion/water complexes that are isolated solvated ions, isolated solvated contact ion pairs, and larger ion/water clusters (tetramers, hexamers, octamers, etc.).[67,84−86] We assume that the dynamics contributing to C_{fast} are from the water solvating the isolated solvated ions and isolated solvated contact ion pairs. Except at the two lowest concentrations studied, there is insufficient water to have structures that resemble those of pure water. The signals from the water solvating ions are ∼2 times larger than that of pure water, although this value is difficult to measure precisely. Therefore, pure water-like structures do not contribute significantly to C_{fast} and are not considered. The simulation results are divided into the fraction: ions that are isolated solvated ions plus isolated solvated contact ion pairs divided by the sum of ions that are isolated solvated ions, isolated solvated contact ion pairs, and larger ion clusters (orange circles), S_{CIP-II}

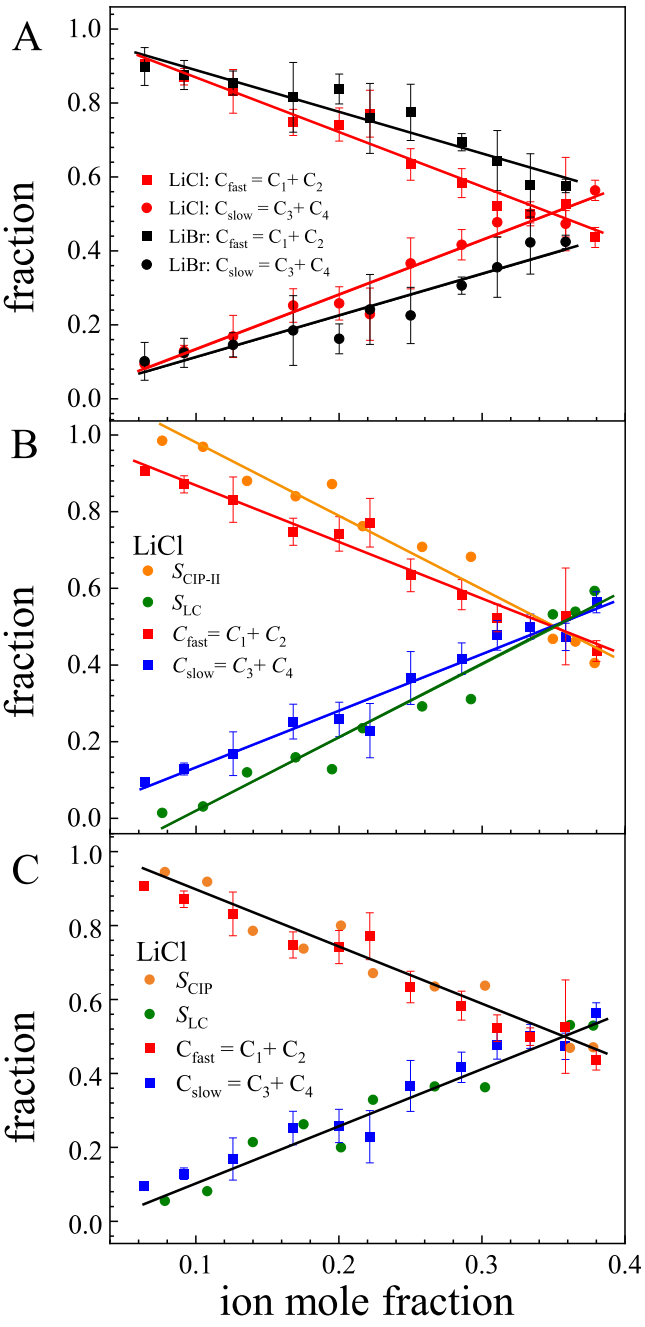

Figure 3. Fractions of the fast and slow portions of the decays from the coefficients of the four exponentials from the fits of the OHD-OKE data. (A) Comparison of the amplitudes (C_{fast} and C_{slow}) as a function of ion mole fraction of LiBr and LiCl in aqueous solutions. LiCl data were obtained from reference.[62] The lines are linear fits to the data. The LiBr and LiCl data show the same trend with different slopes. (B) Relative fractions of fast (C_{fast}) and slow (C_{slow}) decay components in LiCl solutions as a function of the ion mole fraction in water compared to the results of MD simulations of the concentration-dependent structures of LiCl solutions.[67] S_{CIP-II} is the fraction: ions that are solvated isolated contact ion pairs and solvated isolated ions divided by all ions, i.e., solvated isolated ions, solvated isolated contact ion pairs, and large ion clusters. S_{LC} is the fraction: ions that are in large clusters divided by all ions, i.e., solvated isolated ions, solvated isolated contact ion pairs, and large clusters. The agreement between the data and the simulations is good. (C) The same as B except solvated isolated ions are not included. S_{CIP} is the fraction: ions that are solvated isolated contact ion pairs divided by solvated isolated contact ion pairs plus large clusters. S_{LC} is the

https://doi.org/10.1021/acs.jpcb.3c07711
J. Phys. Chem. B 2024, 128, 291−302

Figure 3. continued

fraction: ions that are in large ion clusters divided by solvated isolated contact ion pairs and large clusters. The agreement between the data and the simulations is very good. Both B and C demonstrate that C_{slow} corresponds to the fraction of ions that are large ion clusters.

(contact ion pairs−isolated ions), and the fraction: larger ion/water clusters divided by the sum of ions that are isolated solvated ions, isolated solvated contact ion pairs, and larger ion clusters (green circles) S_{LC} (large clusters).

The experimental fractions C_{fast} and C_{slow} show quite reasonable agreement with the simulated fractions of solvated isolated ions plus solvated contact ion pairs ($S_{CIP\text{-}II}$) and large ion/water clusters (S_{LC}) as a function of the IMF. Therefore, in the LiCl solutions, t_1 and t_2 structural relaxation times can be attributed to the dynamics of isolated ion/water and contact ion pair/water structures, while t_3 and t_4 reflect the dynamics of large ion/water clusters. These results support the division of the time decays into two pairs. The comparison to the simulations shows that the two fast decays and the two slow decays arise from different types of structures. These structures have dynamics that occur on different time scales.

The C_{fast} and C_{slow} data can be compared to the simulations in a different manner. It is possible that the isolated solvated contact ion pairs produce much larger OHD-OKE signals and, therefore, much larger contributions to C_{fast} than solvated isolated ions. Isolated Li^+ and Cl^- ions in the gas phase would generate zero OKE signal. Although they are polarizable, they do not have polarizability anisotropy. However, a contact ion pair would produce a significant OKE signal in the gas phase because it has anisotropic polarizability. In water, the isolated ions are solvated. An Li^+ is solvated by four water molecules. In the ideal case, the oxygens would form a tetrahedral arrangement. For this perfect structure, by symmetry, the solvated Li^+ would produce no OKE signal. However, deviations from a perfect tetrahedral arrangement caused by structural fluctuations would result in an OKE signal. The same is true for Cl^- if it is solvated by six water molecules in a nominal octahedral arrangement. In contrast, a solvated contact ion pair has intrinsically large anisotropic polarizability as the two ends of the pair are solvated in very different manners. Therefore, the solvated contact ion pair may generate far more signal than solvated isolated ions. It is not possible to examine the relative strengths of the signal experimentally. Changing samples and comparing the absolute magnitudes of signals is problematic. In addition, a concentration study has changing contributions from isolated ions, contact ion pairs, and large ion clusters with proportions and time constants changing.

Figure 3C compares the C_{fast} and C_{slow} data and the simulations in which only solvated contact ion pairs and larger ion clusters are considered. In Figure 3C, the simulation results are divided into the fraction: isolated solvated contact ion pairs divided by isolated solvated contact ion pairs plus larger ion clusters (orange circles), S_{CIP} (contact ion pairs), and the fraction: larger ion/water clusters divided by isolated solvated contact ion pairs plus larger ion clusters (green circles) S_{LC} (large clusters). The agreement between C_{fast} and C_{slow} data and the MD simulations[62,67] is very good. The important aspects of both Figure 3B,C are the agreement between the C_{fast} and C_{slow} data and the MD simulations. The agreement shows that C_{slow}, and therefore C_3, C_4, t_3, and t_4 can be associated with large ion clusters, which is necessary for the results presented below. In addition, C_{fast}, and therefore C_1, C_2, t_1, and t_2 can be associated with ions that are not part of large clusters.

The experimental and simulation results shown in Figure 3B,C are for LiCl solutions. The comparison of the LiBr and LiCl concentration-dependent data in Figure 3A shows that C_{fast} and C_{slow} for the two types of salt solutions behave similarly. In addition, the four LiBr time constants (see Figure 2) show identical trends as the four LiCl time constants.[62] Therefore, making the same C_{fast} and C_{slow} structural assignments for LiBr as those done for LiCl is reasonable. There is one caveat. The simulations for LiCl show that the ion pairs are contact ion pairs.[67] There are no equivalent simulations for LiBr. THz absorption experiments in the 200 cm^{-1} range indirectly suggest that ion pairs with Br^{1-} anions, but not specifically LiBr, can be solvent-separated.[87] However, the similarities between the LiBr and LiCl data, including additional results presented below, indicate that the LiBr ion pairs are likely contact ion pairs.

3.2. Concentration-Dependent Dynamics and the Bulk Viscosities. At high salt concentrations, aqueous LiBr and LiCl solutions experience a rapid rise in viscosity, becoming approximately six and ten times more viscous than water, respectively.[69,88] LiCl has a viscosity higher than that of LiBr at every concentration. The C_{slow} component of LiCl solutions also grows with concentration, reflecting the growth of large ion/water clusters. C_{slow} in LiBr solutions increases with concentration in a similar manner (see Figure 3A).

The previous study of LiCl showed that the bulk viscosity is linearly related to the correlation time of the slow dynamics.[62] The correlation time is a single time constant, τ_c, that reflects the overall time scale of dynamical processes:

$$\tau_c = \int_0^\infty f(t)dt \tag{4}$$

For the two slow dynamic components associated with the large ion/water clusters, the correlation time τ_c^{slow} is the weighted average of the two slowest time constants t_3 and t_4:

$$\tau_c^{slow} = C_3 t_3 + C_4 t_4 \tag{5}$$

Figure 4 (see also Tables S4 and S9) shows the bulk viscosities vs the correlation times of the slow dynamics, τ_c^{slow}, for LiBr and LiCl[62] solutions. Both the LiBr and LiCl bulk viscosities are linearly related to the correlation times and fall on the same line. As the ion concentration increases, C_{slow} increases, and both t_3 and t_4 slow. At the low end of the concentration range, $C_3 > C_4$. As the ion concentration increases, both C_3 and C_4 increase, but C_4 increases faster than C_3 (see Table S3). Figure 4 shows that the slow structural relaxation, rather than the fast water-like dynamics, determines the viscosity of both LiBr and LiCl. Even though LiBr is less viscous than LiCl at all concentrations studied, a specific correlation time corresponds to the same viscosity. The large cluster dynamics are determined by both time constants, t_3 and t_4, and the fractions of structural relaxation that occur with each time constant, C_3 and C_4. These dynamics are captured in τ_c^{slow}.

Except at the lowest concentrations studied here (<~4 m), there is insufficient water to fully solvate isolated ions, ion pairs, and a very small number of larger clusters. In the simulations discussed above,[67] clusters are defined as contact ion pairs, ion tetramers, hexamers, octamers, etc. An, e.g.,

https://doi.org/10.1021/acs.jpcb.3c07711
J. Phys. Chem. B 2024, 128, 291−302

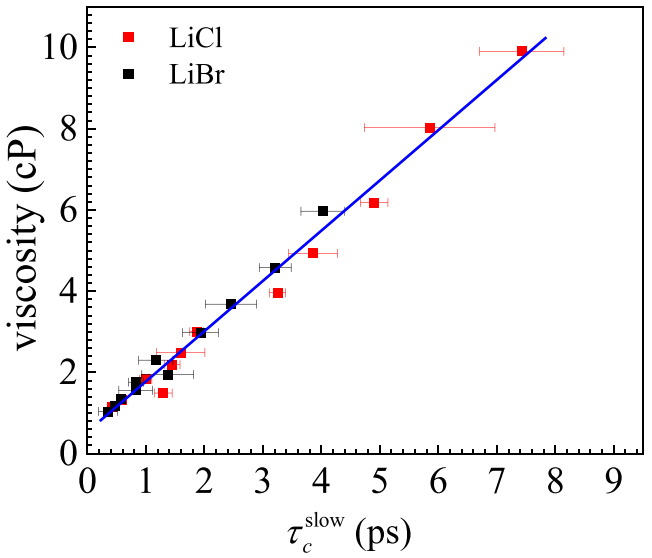

Figure 4. Viscosity as a function of the correlation time of the slow dynamics, τ_c^{slow}, in LiBr and LiCl solutions. The blue line is a concatenated linear fit. The viscosity data for LiBr and LiCl are from reference[69] (see SI). The bulk viscosities as a function of concentration for both LiBr and LiCl are linearly dependent on τ_c^{slow} and fall on the same line.

octamer is defined as eight ions that all have direct contact with two other ions except at the ends, where there can be single ion contact. Because of insufficient water, individual large ion clusters cannot be entirely surrounded by solvation shells of water. Instead, water molecules form bridges among clusters. The ion clusters with bridging waters form a continuous ion/water network. Locally, there will be distinct ion/water structures. The time constants, t_3 and t_4, are the time constants for the relaxation of local ion clusters with bridging waters. There needs to be anisotropic polarizability to generate an OKE signal that decays with t_3 and t_4. The distinct local structures with different numbers of ions, configurations, and orientations will give rise to the necessary anisotropic polarizability. Figure 4 shows that these local relaxations determine the viscosities of high salt concentration LiBr and LiCl solutions.

A rate process theory of viscosity for molecular liquids, which is an activated process, was developed by Raymond and Eyring.[89] The key aspect of this theory is that two molecules exchange places, which requires passing over a potential barrier. When no external stress is applied, a molecule's forward and backward motions are equally likely and there is no net flow. However, when a shear force is applied, the potential barrier is deformed, favoring forward motion and hence flow.

The molecular theory of viscosity is dependent on the existence of individual molecular units. However, reliable methods are lacking to estimate the specific sizes of the clusters in concentrated salt solutions that correspond to individual molecular units. In a concentrated salt solution, there are cations, anions, and water molecules. Rather than discrete molecules or larger structural units, ion clusters are joined by water molecules, forming a dynamic ion/water network. In analogy to Eyring's model, in lieu of molecules, the extended ion network is composed of local ion/water structures. Relaxation of these ion/water structures, driven by thermal fluctuations, is analogous to Eyring's one molecule exchanging places with another.[89] When shear force is applied, the random configurational relaxation of local ion/water clusters is skewed in the forward direction. The local ion/water cluster relaxation is characterized by τ_c^{slow}. Akin to the molecular model, the viscosity of the concentrated salt solutions should be an activated process. In the next section, the temperature-dependent dynamics are considered, including the activation enthalpy of τ_c^{slow} and the relationship of τ_c^{slow} to the temperature-dependent viscosity.

3.3. Temperature-Dependent Dynamics of LiCl Solutions. The temperature dependence of LiCl solutions was studied at two concentrations, 1−6 and 1−10, which correspond to IMFs of 0.25 and 0.16 (9.3 and 5.6 m), respectively. OHD−OKE data were acquired from 15 to 95 °C in ∼10 °C steps. Figure 5A shows some of the decay curves for

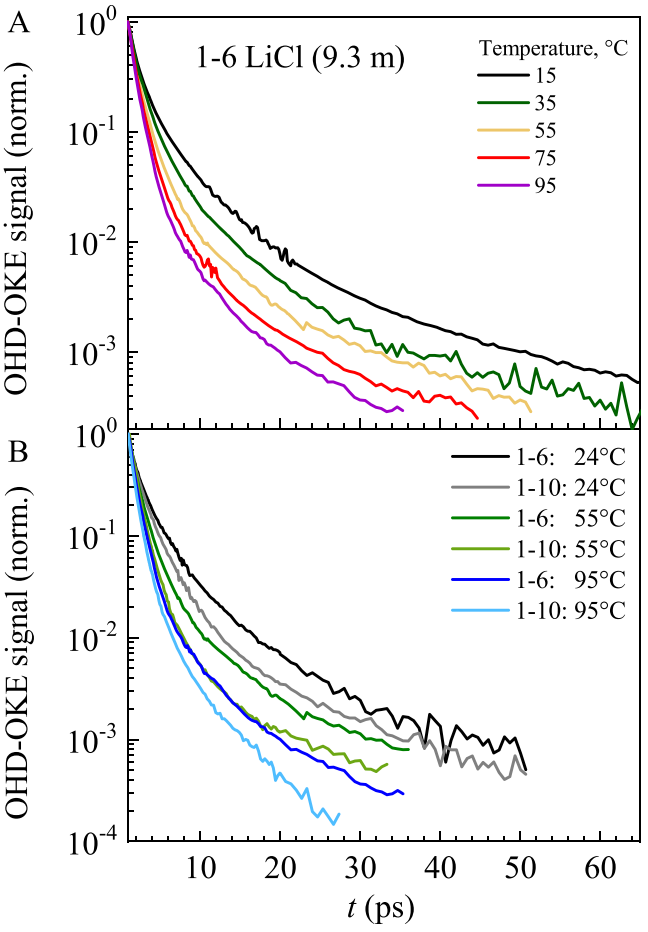

Figure 5. OHD−OKE signal decay of aqueous LiBr and LiCl solutions at different temperatures. The concentrations are given as 1 ion pair-number of water molecules. (A) Subset of OHD−OKE signal decays of 1−6 LiCl solutions at different temperatures. (B) Comparison OHD−OKE signal decays of 1−6 and 1−10 LiCl solutions at various selected temperatures. All of the data are given in the SI.

the 0.25 IMF (1−6). The full set of curves for the 1−6 and 1−10 samples are presented in the SI, Figure S3. Figure 5B compares the decays at several temperatures for the two concentrations.

Figure 6 and Table S5 show the four temperature-dependent time constants for the 1−10 LiCl solution. The 1−6 LiCl solution data are given in the SI, Figure S4 and Table S6. Note

https://doi.org/10.1021/acs.jpcb.3c07711
J. Phys. Chem. B 2024, 128, 291−302

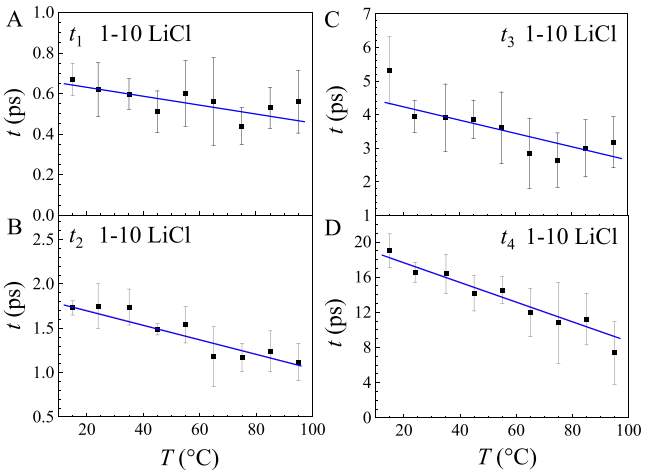

Figure 6. Four time constants, t_1 (A), t_2 (B), t_3 (C), and t_4 (D), from the fits for OHD-OKE data of 1−10 LiCl solutions as a function of temperature. The lines are fits to the data. See SI for the 1−6 data.

that the vertical axes on the four plots differ. The lines, linear fits to the data, are used for comparison, but because of the large error bars, the linearity of the data is not established. The fits show that t_1, t_2, and t_3 decrease by factors of ∼1.5 over the increasing temperature range, while t_4 has a more pronounced change with temperature, a factor of ∼2. The 1−6 data show less change with temperature: t_1, t_2, and t_3, within the noise, show almost no change, while t_4 decreases ∼1.7 times as the temperature increases. The changes in the decay curves with temperature shown in Figure 5 result from changes in both the time constants and the amplitudes (see SI, Tables S7 and S8). As with the concentration dependences discussed above, we divide the amplitudes into two pairs: $C_{fast} = C_1 + C_2$ and $C_{slow} = C_3 + C_4$. Figure 7 displays C_{fast} and C_{slow} for the 1−10 and 1−6 LiCl solutions. As the temperature increases, C_{fast} is approaching 1, and C_{slow} is approaching zero.

Above, it was shown that the concentration-dependent viscosity parallels τ_c^{slow}, the correlation time representing the slow components of the tetra-exponential decay (Figure 4). The linear relation holds for both LiCl and LiBr. The

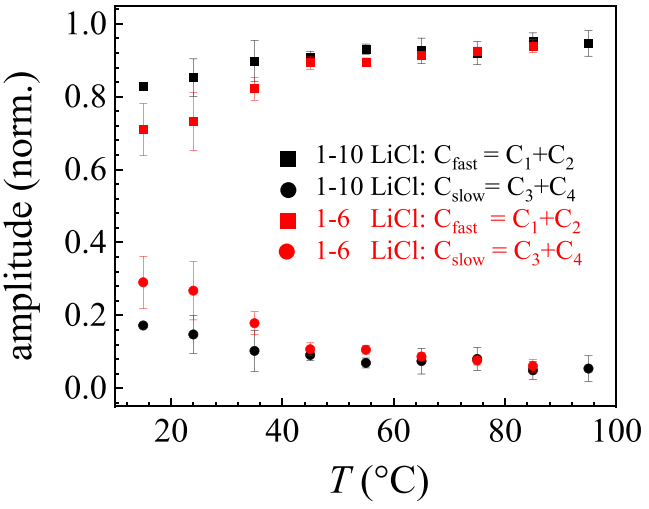

Figure 7. Amplitudes of fast ($C_{fast} = C_1 + C_2$) and slow ($C_{slow} = C_3 + C_4$) decaying components as a function of temperature of 1−10 and 1−6 LiCl solutions.

temperature-dependent viscosities (see SI, Tables S9 and S10)[69,88] for both concentrations (1−6 and 1−10) vs the temperature-dependent τ_c^{slow} are shown in Figure 8. The

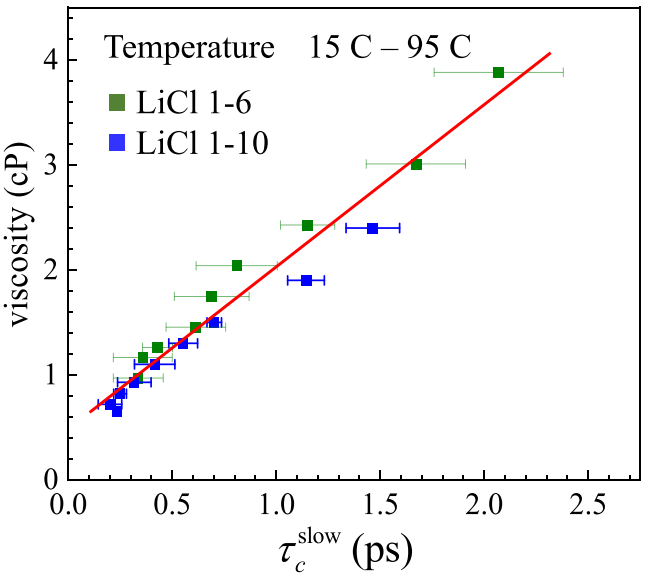

Figure 8. Viscosity as a function of the correlation time of the slow dynamics, τ_c^{slow}, in 1−10 and 1−6 LiCl solutions at different temperatures. The red line is a concatenated linear fit. The viscosity data are from refs 72 and 56 respectively.

temperature-dependent data for the two concentrations are linearly correlated with τ_c^{slow} and fall on the same line within the error. As the temperature increases, the slow correlation time becomes faster and the viscosity decreases. As with the concentration dependence, the viscosity tracks τ_c^{slow}. The temperature-dependent viscosity is determined by the temperature-dependent weighted average of the time constants, corresponding to the overall dynamics of large ion/water clusters. As discussed above, τ_c^{slow} likely describes the relaxation of local clusters embedded in a more extensive ion/water network. The relaxation of these structures controls both the temperature- and concentration-dependent viscosities.

The large ion/water clusters that give rise to τ_c^{slow} determine the concentration dependence of the viscosity for both LiCl and LiBr solutions and the temperature-dependent viscosity of LiCl solutions at the two concentrations studied. Figure 9 shows the relationships between the viscosities and τ_c^{slow} for the LiCl and LiBr concentration and temperature dependences. The inset is an expanded view of the first few picoseconds of τ_c^{slow} in the low-viscosity portion of the plot, which has very dense data. All four data sets fall on the same line, within experimental error. These are notable results: a specific concentration, anion, and temperature give rise to a particular slow correlation time. Regardless of how the correlation time is achieved, a given τ_c^{slow} value is associated with a specific viscosity. At least for LiCl and LiBr solutions over the wide range of concentrations and temperatures studied, knowing τ_c^{slow} and the line in Figure 9 is sufficient information to give the viscosity. In fact, the line in Figure 9 is a calibration curve. Conversely, the value of the viscosity provides τ_c^{slow}, although the viscosity does not give the individual time constants and amplitudes. A temperature decrease has the same effect as an increase in concentration, i.e., increasing the relative

https://doi.org/10.1021/acs.jpcb.3c07711
J. Phys. Chem. B 2024, 128, 291−302

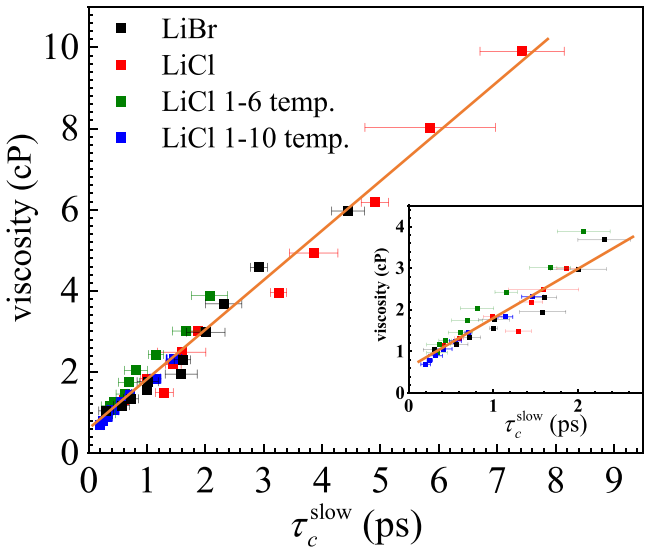

Figure 9. Viscosity as a function of the correlation time of the slow dynamics, τ_c^{slow}, in 1−10 and 1−6 LiCl solutions at different temperatures and LiCl and LiBr data at different concentrations at room temperature. The orange line is a concatenated linear fit. Within experimental error, all four data sets fall on the same line. The viscosity data are from the literature.[88,69]

concentration of large clusters and slowing their time evolution.

As mentioned above, there is a rate process theory predicting the viscosity of molecular liquids based on transition rate theory.[89] $1/\tau_c^{slow}$ is the rate constant for the relaxation of the large ion/water clusters. We can examine its temperature dependence with simple transition rate theory:[68]

$$\frac{1}{\tau_C^{slow}} = \frac{k_B T}{h} e^{-\Delta G*/RT} = \frac{k_B T}{h} e^{-(\Delta H*/RT - T\Delta S*/RT)} \quad (6)$$

where ΔG^* is the activation free energy, ΔH^* is the activation enthalpy, ΔS^* is the activation entropy, R is the gas constant, h is Planck's constant, k_B is Boltzmann's constant, and T is the absolute temperature. Then,

$$\frac{1}{\tau_C^{slow}} = \frac{k_B T}{h} e^{-\Delta H*/RT} e^{\Delta S*/R} \quad (7)$$

$$\ln(\tau_C^{slow})^{-1} - \ln(k_B T/h) = -\Delta H^*/RT + \Delta S^*/R \quad (8)$$

$$\ln[(\tau_C^{slow})^{-1}(h/k_B T)] = -\Delta H^*/RT + \Delta S^*/R \quad (9)$$

If this description of the temperature dependence holds, then a plot of the $1/\tau_c^{slow}$as $\ln[(\tau_C^{slow})^{-1}(h/k_B T)]$ vs $1/RT$ will fall on a line; the slope of the line will give the activation enthalpy, ΔH^*, and the intercept will give the activation entropy, ΔS^*.

Figure 10 shows plots of $(\tau_C^{slow})^{-1}(h/k_B T)$ on a log scale vs $1/RT$ for concentrations 1−10 and 1−6. The data for both concentrations are linear. The term −ln $(k_B T/h)$ changes only mildly over the temperature range. These results strongly suggest that the temperature-dependent relaxation rate of the large ion/water clusters, as embodied in $1/\tau_c^{slow}$, is an activated process. The ΔH^*s for the concentrations 1−10 and 1−6 are 20 and 19 kJ/mol, respectively. Within error, ΔH^* is essentially the same for the two concentrations: ΔH^* = ∼20 or 4.8 kcal/mol. The activation entropies, ΔS^*, are 7.0 ± 0.2

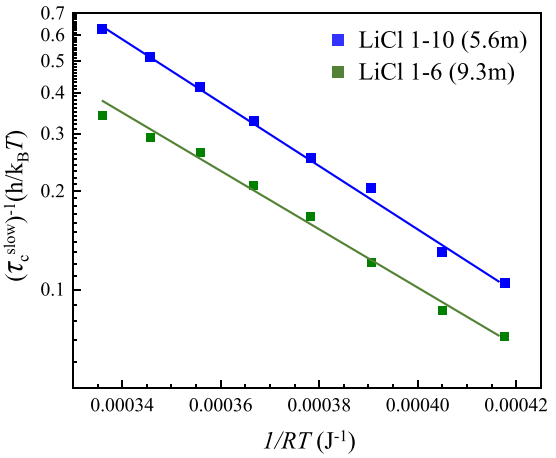

Figure 10. Slow correlation time, τ_c^{slow}, as a function of the temperature plotted as $(\tau_C^{slow})^{-1}(h/k_B T)$ on a log scale vs $1/RT$ for the 1−10 and 1−6 LiCl solutions. The points fall on lines for both concentrations, indicating an exponential activated process, and yield activation enthalpies of 20 and 19 kJ/mol, respectively.

and 5.7 ± 0.3 J/K for 1−10 and 1−6, respectively. The fact that ΔS^* for the lower concentration is larger may be due to the presence of more water molecules. By multiplying by the average temperature, the entropic contribution to the total free energy can be found. These are 2.3 and 1.9 kJ/mol. Therefore, the activation free energy, ΔG^*, is dominated by the change in enthalpy.

4. CONCLUDING REMARKS

We have investigated the concentration-dependent dynamics of LiBr salt solutions using OHD-OKE experiments and compared the results to previous measurements on LiCl solutions[62] over the same high concentration ranges at room temperature (∼24.5 °C). The concentrations extended from the low end with 1 ion pair to 29 water molecules (1−29, 1.9 m) to the high end, 1−3.6 (15.5 m). To form a first solvation shell, a bromide anion or a chloride anion requires ∼6−8 water molecules, and a lithium ion requires 4 water molecules.[90−92] Thus, at the 1−29 ratio, there are still some water molecules not directly solvating an ion. At higher concentrations, there are far too few water molecules to form individual ion solvation shells. The liquid structure is composed of large ion clusters bridged to other clusters by water molecules, forming an extended network.

While the decay of the OHD−OKE signal of pure water is biexponential, all the salt solution data, both temperature- and concentration-dependent, decayed as tetra-exponentials. Separating the total measured polarization correlation function decay into fast (t_1 and t_2) and slow (t_3 and t_4) components with their associated coefficients, $C_{fast} = C_1 + C_2$ and $C_{slow} = C_3 + C_4$, we have shown that the ion/water solutions could be divided into two classes of ion/water structures. The rapid structural relaxation class is composed of solvated contact ion pairs and isolated ions. The slow structural relaxation class is composed of large ion/water clusters. As the concentration is increased or the temperature is decreased, the fraction of large ion/water clusters, C_{slow}, grows at the expense of the solvated contact ion pairs and solvated isolated ions, and the slow time constants (t_3 and t_4) become even slower.

The dynamics of the large ion/water clusters depend on the fractions (C_3 and C_4) and the time constants (t_3 and t_4). To

https://doi.org/10.1021/acs.jpcb.3c07711
J. Phys. Chem. B 2024, 128, 291−302

capture the concentration- and temperature-dependent trends, we investigated the correlation time (see eqs 4 and 5), τ_C^{slow}, which is the fraction-weighted sum of the two slow time constants. An important result is that the bulk viscosities as a function of the concentrations of both LiBr and LiCl, and the LiCl temperature-dependent viscosities for the two concentrations all track τ_C^{slow}, showing that the dynamics and concentrations of the large local structures determine the bulk viscosity. The structural dynamics of the relaxing structures reflected in t_3 and t_4 with the associated C_3 and C_4, determine the viscosity.

The temperature dependence of the slow correlation rate constant, $1/\tau_C^{slow}$, for the two concentrations (1−6 and 1−10) was analyzed with transition state theory (see Figure 10), yielding essentially the same activation enthalpies, ∼20 kJ/mol (4.8 kcal/mol), although the activation entropies differ. It is interesting to consider that there may be a relation between this ΔH^* and the viscosity's activation enthalpy. As discussed briefly above, a rate process theory based on transition state theory for the viscosity of molecular liquids[89] shows that viscosity is an activated process. It was argued that the local ion/water clusters play an analogous role in determining the viscosity of concentrated salt solutions as molecules do in molecular liquids. The strong relationship between the bulk viscosity suggests that the ΔH^* found for the rate $1/\tau_C^{slow}$ may correspond to the viscosity activation energy for these concentrated water-in-salt solutions.

■ ASSOCIATED CONTENT

Data Availability Statement

Data are available by contacting Professor Michael D. Fayer, Department of Chemistry, Stanford University, Stanford, CA 94305-5080. email: fayer@stanford.edu

Supporting Information

The Supporting Information is available free of charge at https://pubs.acs.org/doi/10.1021/acs.jpcb.3c07711.

Viscosity values for 1−10 LiCl solution at various temperatures; full set of OHD-OKE signal decays of various concentrations of aqueous LiBr and LiCl solutions; full set of OHD-OKE signal decays of LiCl solutions at various temperatures; the four temperature-dependent time constants for the 1−6 LiCl solutions; all individual time constants (t_i), amplitudes (C_i, C_{fast}, C_{slow}), and correlation times (τ_C^{slow}) calculated in this study compiled in table format (PDF)

■ AUTHOR INFORMATION

Corresponding Author

Michael D. Fayer − *Department of Chemistry, Stanford University, Stanford, California 94305, United States;* orcid.org/0000-0002-0021-1815; Phone: 650 723-4446; Email: fayer@stanford.edu

Authors

Laura Kacenauskaite − *Department of Chemistry, Stanford University, Stanford, California 94305, United States; Nano-Science Center and Department of Chemistry, University of Copenhagen, Copenhagen 2100, Denmark*

Stephen J. Van Wyck − *Department of Chemistry, Stanford University, Stanford, California 94305, United States;* orcid.org/0000-0001-9011-9977

Max Moncada Cohen − *Department of Chemistry, Stanford University, Stanford, California 94305, United States;* orcid.org/0000-0003-1633-6732

Complete contact information is available at: https://pubs.acs.org/10.1021/acs.jpcb.3c07711

Author Contributions

[§]L.K. and S.J.V.W. contributed equally to this work.

Notes

The authors declare no competing financial interest.

■ ACKNOWLEDGMENTS

This work was supported by the National Science Foundation, Division of Chemistry, Award Number 2319637. L.K. acknowledges support from Villum Fonden (Project No. 41380).

■ REFERENCES

(1) Roedder, E. The Fluids in Salt. *Am. Mineral.* **1984**, *69*, 413−439.
(2) Jungwirth, P.; Cremer, P. S. Beyond Hofmeister. *Nat. Chem.* **2014**, *6*, 261−263.
(3) Oncsik, T.; Trefalt, G.; Borkovec, M.; Szilagyi, I. Specific Ion Effects on Particle Aggregation Induced by Monovalent Salts within the Hofmeister Series. *Langmuir* **2015**, *31*, 3799−3807.
(4) Suo, L.; Borodin, O.; Gao, T.; Olguin, M.; Ho, J.; Fan, X.; Luo, C.; Wang, C.; Xu, K. "Water-in-Salt"; Electrolyte Enables High-Voltage Aqueous Lithium-Ion Chemistries. *Science* **2015**, *350*, 938−943.
(5) Roberts, S. T.; Ramasesha, K.; Tokmakoff, A. Structural Rearrangements in Water Viewed through Two-Dimensional Infrared Spectroscopy. *Acc. Chem. Res.* **2009**, *42*, 1239−1249.
(6) Palese, S.; Schilling, L.; Miller, R. D.; Staver, P. R.; Lotshaw, W. T. Femtosecond Optical Kerr Effect Studies of Water. *J. Phys. Chem.* **1994**, *98*, 6308−6316.
(7) Asbury, J. B.; Steinel, T.; Stromberg, C.; Corcelli, S.; Lawrence, C.; Skinner, J.; Fayer, M. Water Dynamics: Vibrational Echo Correlation Spectroscopy and Comparison to Molecular Dynamics Simulations. *J. Phys. Chem. A* **2004**, *108*, 1107−1119.
(8) Laage, D.; Elsaesser, T.; Hynes, J. T. Water Dynamics in the Hydration Shells of Biomolecules. *Chem. Rev.* **2017**, *117*, 10694−10725.
(9) Guchhait, B.; Liu, Y.; Siebert, T.; Elsaesser, T. Ultrafast Vibrational Dynamics of the DNA Backbone at Different Hydration Levels Mapped by Two-Dimensional Infrared Spectroscopy. *Struct. Dyn.* **2016**, *3*, No. 043202.
(10) Stirnemann, G.; Wernersson, E.; Jungwirth, P.; Laage, D. Mechanisms of Acceleration and Retardation of Water Dynamics by Ions. *J. Am. Chem. Soc.* **2013**, *135*, 11824−11831.
(11) Laage, D.; Stirnemann, G. Effect of Ions on Water Dynamics in Dilute and Concentrated Aqueous Salt Solutions. *J. Chem. Phys. B* **2019**, *123*, 3312−3324.
(12) Hribar, B.; Southall, N. T.; Vlachy, V.; Dill, K. A. How Ions Affect the Structure of Water. *J. Am. Chem. Soc.* **2002**, *124*, 12302−12311.
(13) Bakker, H.; Kropman, M.; Omta, A.; Woutersen, S. Hydrogen-Bond Dynamics of Water in Ionic Solutions. *Phys. Scr.* **2004**, *69*, C14.
(14) Turton, D. A.; Corsaro, C.; Candelaresi, M.; Brownlie, A.; Seddon, K. R.; Mallamace, F.; Wynne, K. The Structure and Terahertz Dynamics of Water Confined in Nanoscale Pools in Salt Solutions. *Faraday Discuss.* **2011**, *150*, 493−504.
(15) Turton, D. A.; Hunger, J.; Hefter, G.; Buchner, R.; Wynne, K. Glasslike Behavior in Aqueous Electrolyte Solutions. *J. Chem. Phys.* **2008**, *128*, 161102.
(16) Wynne, K. The Mayonnaise Effect. *J. Phys. Chem. Lett.* **2017**, *8*, 6189−6192.

(17) Roget, S. A.; Carter-Fenk, K. A.; Fayer, M. D. Water Dynamics and Structure of Highly Concentrated Licl Solutions Investigated Using Ultrafast Infrared Spectroscopy. *J. Am. Chem. Soc.* **2022**, *144*, 4233−4243.
(18) Zhang, Y.; Lewis, N. H. C.; Mars, J.; Wan, G.; Weadock, N. J.; Takacs, C. J.; Lukatskaya, M. R.; Steinrück, H.-G.; Toney, M. F.; Tokmakoff, A.; et al. Water-in-Salt LiTFSi Aqueous Electrolytes. 1. Liquid Structure from Combined Molecular Dynamics Simulation and Experimental Studies. *J. Chem. Phys. B* **2021**, *125*, 4501−4513.
(19) Lewis, N. H. C.; Dereka, B.; Zhang, Y.; Maginn, E. J.; Tokmakoff, A. From Networked to Isolated: Observing Water Hydrogen Bonds in Concentrated Electrolytes with Two-Dimensional Infrared Spectroscopy. *J. Chem. Phys. B* **2022**, *126*, 5305−5319.
(20) Jeon, J.; Cho, M. Ion Transport in Super-Concentrated Aqueous Electrolytes for Lithium-Ion Batteries. *J. Chem. Phys. C* **2021**, *125*, 23622−23633.
(21) Jeon, J.; Lee, H.; Choi, J.-H.; Cho, M. Modeling and Simulation of Concentrated Aqueous Solutions of Litfsi for Battery Applications. *J. Chem. Phys. C* **2020**, *124*, 11790−11799.
(22) Esteves, M. J.; Cardoso, M. J. d. M.; Barcia, O. E. A Debye−Hückel Model for Calculating the Viscosity of Binary Strong Electrolyte Solutions. *Indus. & Eng. Chem. Res.* **2001**, *40*, 5021−5028.
(23) Jiang, J.; Sandler, S. I. A New Model for the Viscosity of Electrolyte Solutions. *Indus. & Eng. Chem. Res.* **2003**, *42*, 6267−6272.
(24) Smith, A. M.; Lee, A. A.; Perkin, S. The Electrostatic Screening Length in Concentrated Electrolytes Increases with Concentration. *J. Phys. Chem. Lett.* **2016**, *7*, 2157−2163.
(25) Yamada, Y.; Usui, K.; Sodeyama, K.; Ko, S.; Tateyama, Y.; Yamada, A. Hydrate-Melt Electrolytes for High-Energy-Density Aqueous Batteries. *Nat. Energy* **2016**, *1*, 16129.
(26) Suo, L.; Borodin, O.; Wang, Y.; Rong, X.; Sun, W.; Fan, X.; Xu, S.; Schroeder, M. A.; Cresce, A. V.; Wang, F. Water-in-Salt" Electrolyte Makes Aqueous Sodium-Ion Battery Safe, Green, and Long-Lasting. *Adv. Energy Mater.* **2017**, *7*, No. 1701189.
(27) Viola, W.; Andrew, T. L. An Aqueous Eutectic Electrolyte for Low-Cost, Safe Energy Storage with an Operational Temperature Range of 150 °C, from − 70 to 80 °C. *J. Chem. Phys. C* **2021**, *125*, 246−251.
(28) Rezaei, M.; Sakong, S.; Groß, A. Molecular Modeling of Water-in-Salt Electrolytes: A Comprehensive Analysis of Polarization Effects and Force Field Parameters in Molecular Dynamics Simulations. *J. Chem. Theory Comput.* **2023**, *19*, 5712−5730.
(29) Chubak, I.; Alon, L.; Silletta, E. V.; Madelin, G.; Jerschow, A.; Rotenberg, B. Quadrupolar $^{23}na^{+}$ Nmr Relaxation as a Probe of Subpicosecond Collective Dynamics in Aqueous Electrolyte Solutions. *Nat. Commun.* **2023**, *14*, 84.
(30) Zhang, C.; Yue, S.; Panagiotopoulos, A. Z.; Klein, M. L.; Wu, X. Dissolving Salt Is Not Equivalent to Applying a Pressure on Water. *Nat. Commun.* **2022**, *13*, 822.
(31) Zhang, C.; Tang, F.; Chen, M.; Xu, J.; Zhang, L.; Qiu, D. Y.; Perdew, J. P.; Klein, M. L.; Xifan Wu, X. Modeling Liquid Water by Climbing up Jacob's Ladder in Density Functional Theory Facilitated by Using Deep Neural Network Potentials. *J. Phys. Chem. B* **2021**, *125*, 11444−11456.
(32) Gibbard, H. F., Jr.; Scatchard, G. Liquid-Vapor Equilibrium of Aqueous Lithium Chloride, from 25 to 100 C and from 1.0 to 18.5 Molal, and Related Properties. *J. Chem. & Eng. Data* **1973**, *18*, 293−298.
(33) Terpstra, P.; Combes, D.; Zwick, A. Effect of Salts on Dynamics of Water: A Raman Spectroscopy Study. *J. Chem. Phys.* **1990**, *92*, 65−70.
(34) Heisler, I. A.; Meech, S. R. Low-Frequency Modes of Aqueous Alkali Halide Solutions: Glimpsing the Hydrogen Bonding Vibration. *Science* **2010**, *327*, 857−860.
(35) Shalit, A.; Ahmed, S.; Savolainen, J.; Hamm, P. Terahertz Echoes Reveal the Inhomogeneity of Aqueous Salt Solutions. *Nat. Chem.* **2017**, *9*, 273−278.
(36) Tao, N. J.; Li, G.; Chen, X.; Du, W. M.; Cummins, H. Z. Low-Frequency Raman-Scattering Study of the Liquid-Glass Transition in Aqueous Lithium Chloride Solutions. *Phys. Rev. A* **1991**, *44*, 6665−6676.
(37) Balos, V.; Kaliannan, N. K.; Elgabarty, H.; Wolf, M.; Kühne, T. D.; Sajadi, M. Time-Resolved Terahertz−Raman Spectroscopy Reveals That Cations and Anions Distinctly Modify Intermolecular Interactions of Water. *Nat. Chem.* **2022**, *14*, 1031−1037.
(38) Tao, N. J.; Lindsay, S. M. Reorientational Relaxation of Water Molecules in Licl Solution Studied by Depolarised Rayleigh Scattering. *J. Phys.: Condens. Matter* **1989**, *1*, 8709−8720.
(39) Chizhik, B. V. I. Nmr Relaxation and Microstructure of Aqueous Electrolyte Solutions. *Mol. Phys.* **1997**, *90*, 653−660.
(40) Harsányi, I.; Pusztai, L. On the Structure of Aqueous Licl Solutions. *J. Chem. Phys.* **2005**, *122*, 124512.
(41) Buchner, R.; Hefter, G. Interactions and Dynamics in Electrolyte Solutions by Dielectric Spectroscopy. *Phys. Chem. Chem. Phys.* **2009**, *11*, 8984−8999.
(42) Wachter, W.; Fernandez, Š.; Buchner, R.; Hefter, G. Ion Association and Hydration in Aqueous Solutions of Licl and Li_2so_4 by Dielectric Spectroscopy. *J. Chem. Phys. B* **2007**, *111*, 9010−9017.
(43) Barthel, J.; Hetzenauer, H.; Buchner, R. Dielectric Relaxation of Aqueous Electrolyte Solutions Ii. Ion-Pair Relaxation of 1:2, 2:1, and 2:2 Electrolytes. *Ber. der Buns. fur Phys. Chem.* **1992**, *96*, 1424−1432.
(44) Yuan, R.; Yan, C.; Fayer, M. Ion−Molecule Complex Dissociation and Formation Dynamics in Licl Aqueous Solutions from 2D IR Spectroscopy. *J. Chem. Phys. B* **2018**, *122*, 10582−10592.
(45) Yuan, R.; Fayer, M. D. Dynamics of Water Molecules and Ions in Concentrated Lithium Chloride Solutions Probed with Ultrafast 2D IR Spectroscopy. *J. Chem. Phys. B* **2019**, *123*, 7628−7639.
(46) Heinzinger, K.; Vogel, P. C. A Molecular Dynamics Study of Aqueous Solutions I. First Results for Licl in H_2O. *Zeit. fur Nat. A* **1974**, *29*, 1164−1171.
(47) Roget, S. A.; Heck, T. R.; Carter-Fenk, K. A.; Fayer, M. D. Ion/Water Network Structural Dynamics in Highly Concentrated Lithium Chloride and Lithium Bromide Solutions Probed with Ultrafast Ir Spectroscopy. *J. Phys. Chem. B* **2023**, *127*, 4532−4543.
(48) Lewis, N. H.; Fournier, J. A.; Carpenter, W. B.; Tokmakoff, A. Direct Observation of Ion Pairing in Aqueous Nitric Acid Using 2D Infrared Spectroscopy. *J. Chem. Phys. B* **2019**, *123*, 225−238.
(49) Horwitz, G.; Härk, E.; Steinberg, P. Y.; Cavalcanti, L. P.; Risse, S.; Corti, H. R. The Nanostructure of Water-in-Salt Electrolytes Revisited: Effect of the Anion Size. *ACS Nano* **2021**, *15*, 11564−11572.
(50) Dubouis, N.; France-Lanord, A.; Brige, A.; Salanne, M.; Grimaud, A. Anion Specific Effects Drive the Formation of Li-Salt Based Aqueous Biphasic Systems. *J. Chem. Phys. B* **2021**, *125*, 5365−5372.
(51) Collins, K. D. Charge Density-Dependent Strength of Hydration and Biological Structure. *Biophys. J.* **1997**, *72*, 65−76.
(52) Crozier, P. S.; Rowley, R. L.; Henderson, D. Molecular-Dynamics Simulations of Ion Size Effects on the Fluid Structure of Aqueous Electrolyte Systems between Charged Model Electrodes. *J. Chem. Phys.* **2001**, *114*, 7513−7517.
(53) Chowdhuri, S.; Chandra, A. Dynamics of Halide Ion−Water Hydrogen Bonds in Aqueous Solutions: Dependence on Ion Size and Temperature. *J. Chem. Phys. B* **2006**, *110*, 9674−9680.
(54) Du, H.; Rasaiah, J. C.; Miller, J. D. Structural and Dynamic Properties of Concentrated Alkali Halide Solutions: A Molecular Dynamics Simulation Study. *J. Chem. Phys. B* **2007**, *111*, 209−217.
(55) Fennell, C. J.; Bizjak, A.; Vlachy, V.; Dill, K. A. Ion Pairing in Molecular Simulations of Aqueous Alkali Halide Solutions. *J. Chem. Phys. B* **2009**, *113*, 6782−6791.
(56) Lyashchenko, A. K.; Zasetsky, A. Y. Complex Dielectric Permittivity and Relaxation Parameters of Concentrated Aqueous Electrolyte Solutions in Millimeter and Centimeter Wavelength Ranges. *J. Mol. Liq.* **1998**, *77*, 61−75.
(57) Amo, Y.; Tominaga, Y. Dynamical Structure of Water in Aqueous Solutions of Licl, Nacl, and Kcl by Low-Frequency Raman Scattering: Comparison between the Multiple Random Telegraph Model and Cole-Cole Relaxation. *Phys. Rev. E* **1998**, *58*, 7553−7560.

https://doi.org/10.1021/acs.jpcb.3c07711
J. Phys. Chem. B 2024, 128, 291−302

(58) Wang, J.; Zheng, Q.; Fang, M.; Ko, S.; Yamada, Y.; Yamada, A. Concentrated Electrolytes Widen the Operating Temperature Range of Lithium-Ion Batteries. *Adv. Sci.* **2021**, *8*, No. 2101646.
(59) Liao, M.; Ji, X.; Cao, Y.; Xu, J.; Qiu, X.; Xie, Y.; Wang, F.; Wang, C.; Xia, Y. Solvent-Free Protic Liquid Enabling Batteries Operation at an Ultra-Wide Temperature Range. *Nat. Commun.* **2022**, *13*, 6064.
(60) Droguet, L.; Grimaud, A.; Fontaine, O.; Tarascon, J. M. Water-in-Salt Electrolyte (Wise) for Aqueous Batteries: A Long Way to Practicality. *Adv. Energy Mater.* **2020**, *10*, No. 2002440.
(61) Hou, M.; Lu, R.; Yu, A. Polarizability Series of Aqueous Polyatomic Anions Revealed by Femtosecond Kerr Effect Spectroscopy. *RSC Adv.* **2014**, *4*, 23078−23083.
(62) Van Wyck, S. J.; Fayer, M. D. Dynamics of Concentrated Aqueous Lithium Chloride Solutions Investigated with Optical Kerr Effect Experiments. *J. Chem. Phys. B* **2023**, *127*, 3488−3495.
(63) Van Wyck, S. J.; Fayer, M. D. Dynamics of Acrylamide Hydrogels, Polymers, and Monomer in Water Measured with Optical Heterodyne Detected Optical Kerr Effect Spectroscopy. *J. Phys. Chem. B* **2023**, *127*, 1276−1286.
(64) Heisler, I. A.; Mazur, K.; Meech, S. R. Low-Frequency Modes of Aqueous Alkali Halide Solutions: An Ultrafast Optical Kerr Effect Study. *J. Chem. Phys. B* **2011**, *115*, 1863−1873.
(65) Turton, D. A.; Corsaro, C.; Martin, D. F.; Mallamace, F. K. W. The Dynamic Crossover in Water Does Not Require Bulk Water. *Phys. Chem. Chem. Phys.* **2012**, *14*, 8067−8073.
(66) Carey, D. M.; Korenowski, G. M. Measurement of the Raman Spectrum of Liquid Water. *J. Chem. Phys.* **1998**, *108*, 2669−2675.
(67) Singh, B. M.; Dalvi, H. V.; Gaikar, G. V. Investigations of Clustering of Ions and Diffusivity in Concentrated Aqueous Solutions of Lithium Chloride by Molecular Dynamic Simulations. *RSC Adv.* **2015**, *5*, 15328−15337.
(68) McQuarrie, D. A.; Simon, J. D. *Physical Chemistry: A Molecular Approach*; University science Books: Sausalito, CA, 1997.
(69) Mao, S.; Duan, Z. The Viscosity of Aqueous Alkali-Chloride Solutions up to 623 k, 1,000 bar, and High Ionic Strength. *Int. J. Thermophys.* **2009**, *30*, 1510−1523.
(70) Fecko, C.; Eaves, J.; Tokmakoff, A. Isotropic and Anisotropic Raman Scattering from Molecular Liquids Measured by Spatially Masked Optical Kerr Effect Spectroscopy. *J. Chem. Phys.* **2002**, *117*, 1139−1154.
(71) Sha, M.; Yamada, S. A.; Fayer, M. D. Orientational Pair Correlations and Local Structure of Benzonitrile from Molecular Dynamics Simulations with Comparisons to Experiments. *J. Chem. Phys. B* **2021**, *125*, 3163−3177.
(72) Deeg, F. W.; Stankus, J. J.; Greenfield, S. R.; Newell, V. J.; Fayer, M. D. Anisotropic Reorientational Relaxation of Biphenyl: Transient Grating Optical Kerr Effect Measurements. *J. Chem. Phys.* **1989**, *90*, 6893−6902.
(73) Ruhman, S.; Williams, L. R.; Joly, A. G.; Kohler, B.; Nelson, K. A. Nonrelaxational Inertial Motion in Carbon Disulfide Liquid Observed by Femtosecond Time-Resolved Impulsive Stimulated Scattering. *J. Phys. Chem.* **1987**, *91*, 2237−2240.
(74) Yan, Y. X.; Nelson, K. A. Impulsive Stimulated Light Scattering. I. General Theory. *J. Chem. Phys.* **1987**, *87*, 6240−6256.
(75) Chandler, D. *Introduction to Modern Statistical Mechanics*; Oxford University Press: New York, 1987.
(76) Sturlaugson, A. L.; Arima, A. Y.; Bailey, H. E.; Fayer, M. D. Orientational Dynamics in a Lyotropic Room Temperature Ionic Liquid. *J. Chem. Phys. B* **2013**, *117*, 14775−14784.
(77) Sturlaugson, A. L.; Fruchey, K. S.; Fayer, M. D. Orientational Dynamics of Room Temperature Ionic Liquid/Water Mixtures: Water-Induced Structure. *J. Chem. Phys. B* **2012**, *116*, 1777−1787.
(78) Chang, Y. J.; Castner, E. W., Jr Fast Responses from "Slowly Relaxing" Liquids: A Comparative Study of the Femtosecond Dynamics of Triacetin, Ethylene Glycol, and Water. *J. Chem. Phys.* **1993**, *99*, 7289−7299.
(79) Winkler, K.; Lindner, J.; Bürsing, H.; Vöhringer, P. Ultrafast Raman-Induced Kerr-Effect of Water: Single Molecule Versus Collective Motions. *J. Chem. Phys.* **2000**, *113*, 4674−4682.
(80) Scodinu, A.; Fourkas, J. T. Comparison of the Orientational Dynamics of Water Confined in Hydrophobic and Hydrophilic Nanopores. *J. Chem. Phys. B* **2002**, *106*, 10292−10295.
(81) Asbury, J. B.; Steinel, T.; Kwak, K.; Corcelli, S. A.; Lawrence, C. P.; Skinner, J. L.; Fayer, M. D. Dynamics of Water Probed with Vibrational Echo Correlation Spectroscopy. *J. Chem. Phys.* **2004**, *121*, 12431−12446.
(82) Yan, C.; Kramer, P. L.; Yuan, R.; Fayer, M. D. Water Dynamics in Polyacrylamide Hydrogels. *J. Am. Chem. Soc.* **2018**, *140*, 9466−9477.
(83) Shannon, R. D. Revised Effective Ionic Radii and Systematic Studies of Interatomic Distances in Halides and Chalcogenides. *Acta Cryst. A: Cryst. Phys. Diff., Theor., and Gen. Cryst.* **1976**, *32*, 751−767.
(84) Hassan, S. A. Computer Simulation of Ion Cluster Speciation in Concentrated Aqueous Solutions at Ambient Conditions. *J. Chem. Phys. B* **2008**, *112*, 10573−10584.
(85) Chen, A. A.; Pappu, R. V. Quantitative Characterization of Ion Pairing and Cluster Formation in Strong 1:1 Electrolytes. *J. Chem. Phys. B* **2007**, *111*, 6469−6478.
(86) Schwaab, G.; Sebastiani, F.; Havenith, M. Ion Hydration and Ion Pairing as Probed by Thz Spectroscopy. *Angew. Chem., Int. Ed.* **2019**, *58*, 3000−3013.
(87) Schwaab, G.; Sebastiani, F.; Martina, H. Ion Hydration and Ion Pairing as Probed by Thz Spectroscopy. *Angew. Chem., Int. Ed.* **2019**, *58*, 3000−3013.
(88) Rohman, N.; Dass, N. N.; Mahiuddin, S. Isentropic Compressibility, Effective Pressure, Classical Sound Absorption and Shear Relaxation Time of Aqueous Lithium Bromide, Sodium Bromide and Potassium Bromide Solutions. *J. Mol. Liq.* **2002**, *100*, 265−290.
(89) Raymond, H. E.; Eyring, H. Theory of the Viscosity of Liquids as a Function of Temperature and Pressure. *J. Chem. Phys.* **1937**, *5*, 726−736.
(90) Ohtaki, H.; Radnai, T. Structure and Dynamics of Hydrated Ions. *Chem. Rev.* **1993**, *93*, 157−1204.
(91) Powell, D. H.; Neilson, G. W.; Enderby, J. E. The Structure of Cl^- in Aqueous Solution: An Experimental Determination of gClH(r) and gClO(r). *J. Phys.: Condens. Matter* **1993**, *5*, 5723−5730.
(92) Antalek, M.; Pace, E.; Hedman, B.; Hodgson, K. O.; Chillemi, G.; Benfatto, M.; Sarangi, R.; Frank, P. Solvation Structure of the Halides from X-Ray Absorption Spectroscopy. *J. Chem. Phys.* **2016**, *145*, No. 044318.

https://doi.org/10.1021/acs.jpcb.3c07711
J. Phys. Chem. B 2024, 128, 291−302